International Journal of Mass Spectrometry 308 (2011) 26–34

Contents lists available at ScienceDirect

International Journal of Mass Spectrometry

journal homepage: www.elsevier.com/locate/ijms

An ion trap CIMS instrument for combined measurements of atmospheric OH and H_2SO_4: First test measurements above and inside the planetary boundary layer

Heinfried Aufmhoff[a,b,*], Markus Hanke[b,1], Jens Uecker[b,2], Hans Schlager[a], Frank Arnold[b,a]

[a] Deutsches Zentrum für Luft- und Raumfahrt, Institut für Physik der Atmosphäre, Oberpfaffenhofen, Germany
[b] Max Planck Institute for Nuclear Physics, Heidelberg, Germany

ARTICLE INFO

Article history:
Received 8 March 2011
Received in revised form 12 July 2011
Accepted 12 July 2011
Available online 21 July 2011

Keywords:
Sulfuric acid
OH
secondary aerosol formation
Chemical ionization
Ion trap

ABSTRACT

Gaseous sulfuric acid (GSA) plays an important role in atmospheric secondary aerosol formation. To quantify its contribution to these processes long-term measurements of GSA using a very sensitive detection method are required. OH is the most important oxidant in the atmosphere and oxidizes, e.g., SO_2. A powerful detection method is chemical ionization mass spectrometry (CIMS). We have built a novel CIMS instrument composed of an ion trap mass spectrometer (ITMS) and a selective ion source suitable to measure gaseous H_2SO_4 and OH and to do fragmentation studies. The probe air inlet and sampling line were optimized to minimize wall losses of H_2SO_4 and OH. An ion source was developed to minimize artificial signals and to create reagent ions ($NO_3^-(HNO_3)_h(H_2O)_n$) which react highly selectively with GSA. An H_2SO_4/OH calibration source based on water vapor photolysis was developed to overcome uncertainties in remaining wall losses, ion residence time, reaction rate coefficient and mass discrimination. Field measurements of GSA in the planetary boundary layer (several weeks at northern and middle latitudes) and high-altitude mountain-site measurements of GSA and OH were carried out. The ITMS instrument offers a detection limit as low as 1×10^5 molecules per cm^3 and a time resolution of about 2 min .

1. Introduction

Atmospheric aerosol particles have a strong influence on Earth's climate and human health. They scatter sunlight, serve as water vapor condensation nuclei (CCN) in cloud formation and thereby change the properties of clouds. In addition certain aerosols also represent major atmospheric pollutants. Several field campaigns [1,2] have implicated that newly formed particles from atmospheric nucleation events are an important source of CCN. To understand the processes which lead to secondary aerosol production, measurements of aerosol precursor gases are required.

Major precursor candidates for nucleation in the atmosphere are gaseous sulfuric acid and water; ammonia as a principal stabilizer of H_2SO_4–H_2O clusters can enhance the H_2SO_4–H_2O nucleation ([3] and references given there). Other bases in the atmosphere besides ammonia are amines. They are also likely to enhance sulfuric acid–water nucleation [4]. Ion clusters (containing H_2SO_4 and H_2O) may also contribute to nucleation in the atmosphere ([5] and references given there, e.g., [6]).

The OH-induced production of H_2SO_4 from the reaction of SO_2 proceeds via the following reaction sequence:

$$OH + SO_2 + M \rightarrow HSO_3 + M \quad (1)$$

$$HSO_3 + O_2 \rightarrow SO_3 + HO_2 \quad (2)$$

$$SO_3 + 2H_2O \rightarrow H_2SO_4 + H_2O. \quad (3)$$

Importantly, OH can be recycled via the reaction

$$HO_2 + NO \rightarrow OH + NO_2. \quad (4)$$

Therefore, in most atmospheric conditions OH acts only as a catalyst and is not consumed by the SO_2-conversion. The first two steps (1) and (2) of the above scheme for OH-induced conversion to gaseous H_2SO_4 was originally proposed by [7]. However, it was not before 1993 that the final step (3) could be proven in the laboratory [8,9]. These laboratory measurements demonstrated that an H_2SO_4 molecule is actually formed and that 2 H_2O molecules are involved in reaction (3). Also they yielded the first quantitative measurement of the rate coefficient of (3). Hereafter, additional laboratory measurements [10,11] confirmed the findings of [8,9].

The production of OH is initiated by the photolysis of O_3 to produce $O(^1D)$. The reaction of $O(^1D)$ with H_2O is the principal source of OH radicals in the troposphere [12].

In this work we present a detailed description of an ITCIMS instrument and its first use in combined measurements of H_2SO_4

* Corresponding author at: Deutsches Zentrum für Luft- und Raumfahrt, Institut für Physik der Atmosphäre, Oberpfaffenhofen, Germany.
E-mail address: Heinfried.Aufmhoff@dlr.de (H. Aufmhoff).
[1] Now at: General Electric, Garching, Germany.
[2] Now at: Siemens AG, Erlangen, Germany.

1387-3806/$ – see front matter © 2011 Elsevier B.V. All rights reserved.
doi:10.1016/j.ijms.2011.07.016

and OH. Previously, several papers have been published presenting data obtained by this instrument but with only limited instrumental information. More data obtained using this instrument are presented here. Detection and quantification of sulfuric acid in the gas phase in the atmosphere have only been possible recently by PACIMS [13–15] and by active CIMS (e.g., [16–20]). We used for the first time an ion trap mass spectrometer (ITMS) for these measurements. An ITMS has also been recently used by DLR (Deutsches Zentrum für Luft- und Raumfahrt)/MPIK (Max Planck Institute for Nuclear Physics) for airborne CIMS measurements of SO_2 [21,22] and PAN [23].

The advantages of ITMS compared to a linear quadrupole mass spectrometer are the possibility of identification of ions via mass selected ion fragmentation [24], a wide mass range (up to 4000 amu/z) at unit resolution and a large sensitivity also at large mass numbers. The relatively large product mass 160 amu ($HSO_4^-HNO_3$) used for the detection of sulfuric acid has been fragmentated with ITMS in the laboratory yielding mass 97 amu (HSO_4^-) which is a verification for this detection method.

At the Environmental Research Station Schneefernerhaus UFS (mountainside Zugspitze, Germany) also simultaneous measurements of GSA and OH with an ITMS via titration of OH with isotopically labeled SO_2 were carried out. The results of these measurements are presented in Section 3.2.

2. Measurement method

The principle ion molecule reaction for the detection of gaseous sulfuric acid by CIMS in the atmosphere with a mass spectrometer was introduced by MPIK Heidelberg [13]. A further development of the PACIMS (passive CIMS)-method described in there (using ambient ions as reagent ions) is the active CIMS method. Reagent ions are introduced into a flow tube by an ion source and react with a rate coefficient k for a given ion residence time t_{ir} with H_2SO_4 while being carried from the ion source to the mass spectrometer.

The ITCIMS instrument (Fig. 1) is composed of 5 major components. These include: an ion source (IS), an ion flow reactor (IFR), an ion trap mass spectrometer (ITMS), a sampling line (SL) and an H_2SO_4/OH calibration source (CS). In the following subsections, these components will be individually discussed.

Also for OH measurements, the detection of H_2SO_4 is utilized by ITCIMS. For OH, artificial H_2SO_4 is produced via titration with isotopically labeled $^{34}SO_2$. For more details see Section 3.2. In Sections 2.1 and 2.2 it is not distinguished between ambient and artificial H_2SO_4 because it is assumed that both, $H_2{}^{32}SO_4$ and $H_2{}^{34}SO_4$ react chemically in the same way with the reagent ions produced in the IS.

The calibration of GSA and OH measurements are based on the production of a certain concentration of OH radicals (see Section 2.5) and the subsequent titration with $^{32}SO_2$. It is important to note that the titration in all cases occurs just after the probe air inlet to avoid competing losses of the OH radicals.

2.1. Ion source

The reagent ions are produced in a capillary ion source (IS) (see Fig. 1). The casing of the ion source was constructed from stainless steel parts and an aluminium rod to fix the sealed radioactive source Po-210 (P-2042 Nuclespot, maximal activity 185 MBq, NRD inc.). The ionization is caused by the alpha particle emitter Po-210. Primary ions (ion pairs) are produced in the part of the ion source case with distance a and diameter 4 cm in a HNO_3/N_2-mixture (≈0.2 μmol/mol in 2–3 slm N_2 5.0). This mixture is produced with a permeation tube (e.g., HRT-10.00 2022/50 Kin-Tek, alternatively Dynacel) and a permeation oven (MK5 special, MCZ).

The distance a was optimized for maximum net ion production and was found to be about 1 cm for a source with the maximum activity of 185 MBq. This distance a is far less than the range of α-particles (3–4 cm). Most likely, ion recombination and eventually wall losses of ions are the reasons that a higher distance a leads to a lower net ion production. The subsequent ion evolution leads to the desired NO_3^--ions due to processes similar to those in the atmosphere. HNO_3 reacts with negative precursor ions to form NO_3^- [25,26]. To more than 90% of the NO_3^--ions at least one HNO_3-molecule is attached (see Fig. 2). Hence $NO_3^-HNO_3(H_2O)_n$ and most likely $NO_3^-(HNO_3)_2(H_2O)_n$ are the effective reagent ions for H_2SO_4 detection (the hydrates and most of the second HNO_3-ligands are not visible as these ligands are detached from the ions in the ion trap by collisions with helium atoms). There is a risk of artificial H_2SO_4 formation by OH and HO_2 radicals formed in the ion source and the SO_2 introduced into the sampling line SL (SO_2 for the titration and SO_2 from the probe air). In order to remove these undesired ion source generated radicals, NO_2 (2.5 mmol/mol in 2–3 slm N_2 5.0 from a gas cylinder) was introduced as a scavenging gas which converts these radicals to HNO_3. The reagent ions are introduced into the flow tube reactor IFR where the ion molecule reactions with atmospheric gases take place.

2.2. Ion molecule reactions

The reactions are assumed to be of pseudo first order and therefore the concentration of H_2SO_4 is proportional to $1/kt_{ir} \times \ln(1+R)$, with R: ratio of product and reagent ions. The overall reaction scheme with H_2SO_4 and the core ion NO_3^- reacting to the core ion HSO_4^- and HNO_3 is:

$$\begin{aligned} &NO_3^-(HNO_3)_h(H_2O)_n + H_2SO_4 \rightarrow \\ &HSO_4^-(HNO_3)_l(H_2O)_m + (h-l+1)HNO_3 + (n-m)H_2O. \end{aligned} \quad (5)$$

The corresponding rate coefficients $k_{h,n}$ have been measured for $h = 0-3$ ($n = 0$) and $n = 0-3$ ($h = 0$) by [27]. For (h, n)= (0,0), (1,0), (2,0) the rate coefficients are:

$$\begin{aligned} k_{h,0} &= 2.32 \times 10^{-9} cm^3/s \,(h=0), \\ &= 1.86 \times 10^{-9} cm^3/s \,(h=1), \\ &= 1.72 \times 10^{-9} cm^3/s \,(h=2), \end{aligned} \quad (6)$$

with relative errors between plus or minus 10 and 15%. Reaction (5) is a fast exothermic proton transfer reaction with rate coefficients close to the collision rates. A strong temperature dependence is not expected for such reactions. The influence on the rate coefficients $k_{1,n}$ is not significant [28]. There is no significant water vapor dependence of the ion molecule reaction scheme used for the detection of gaseous sulfuric acid as has been empirically shown by the MPIK group. However, there is a water vapor dependency of the sensitivity of the ion trap mass spectrometer ITMS. The transmission of large cluster ions is smaller than the transmission of unhydrated core ions. But this effect does not influence the accuracy of the sulfuric acid measurements, because CIMS is based on the detection of the ratio of product and reagent ions and not on absolute ion count rates.

The ion molecule reactions take place in the ion flow reactor IFR (QF40 stainless steel, diameter 4 cm, length ≈ 0.4 m) at atmospheric pressure p and controlled temperature T_I (heating tapes). T_I was chosen between 32 °C and 37 °C. These temperatures are too low to vaporize significant amounts of sulfuric acid from aerosol particles, but high enough to lower the relative humidity in IFR and thus enhance the sensitivity of ITMS [29].

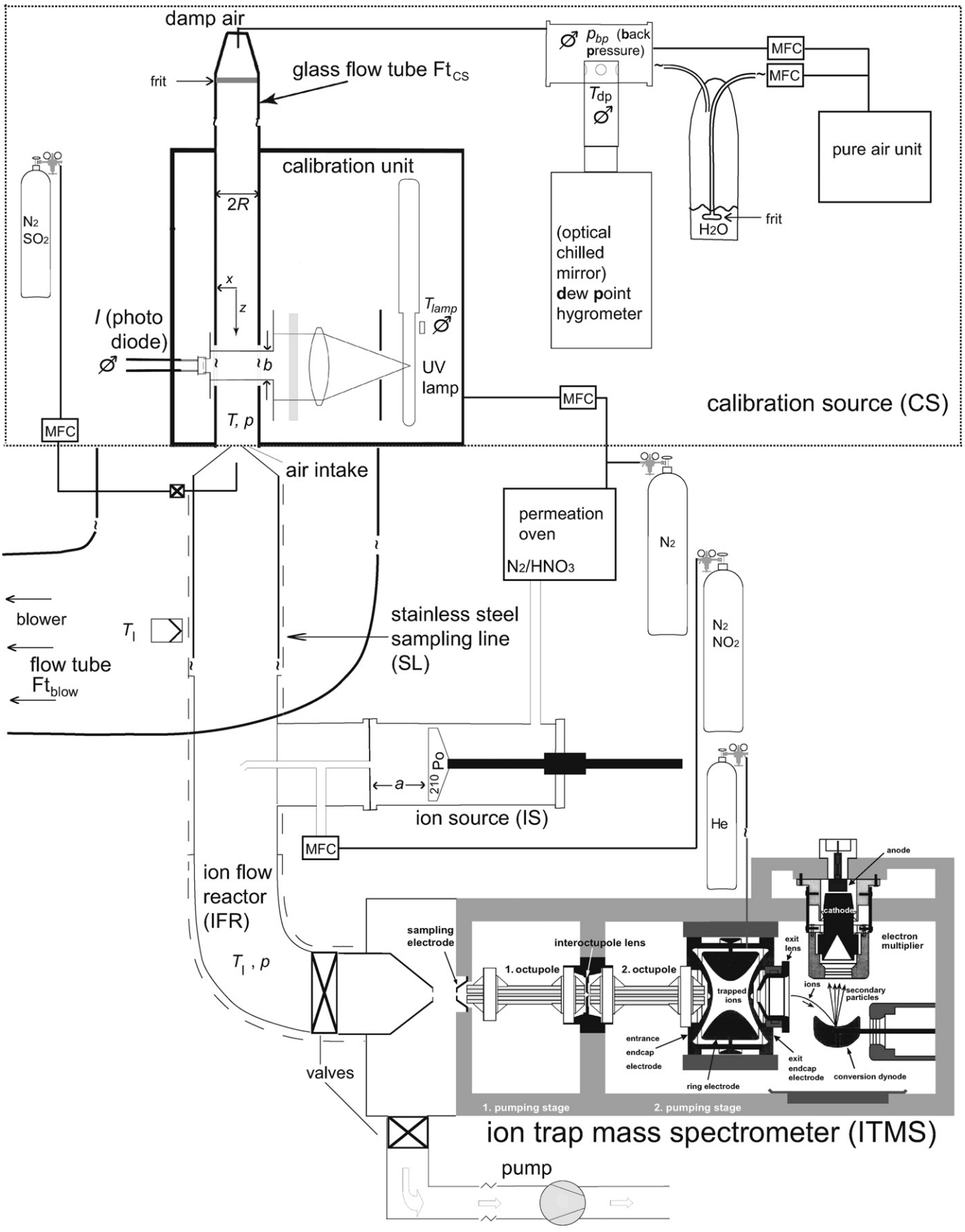

Fig. 1. Setup for atmospheric measurements of GSA and OH with ITCIMS and calibration source. MFC: thermal mass flow controller

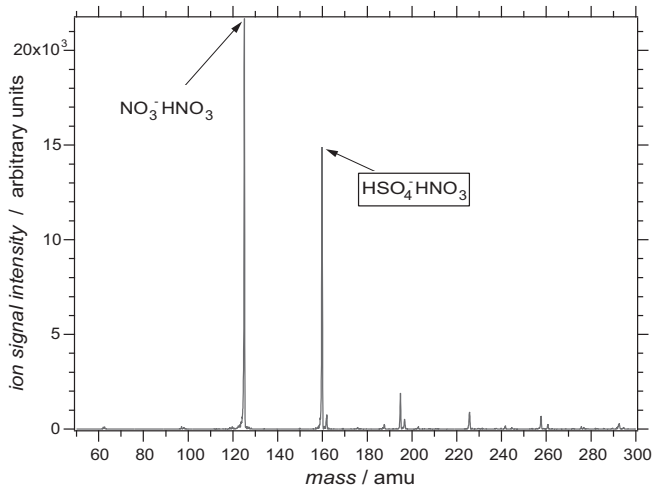

Fig. 2. Mass spectrum obtained with calibration source (CS).

2.3. Ion trap mass spectrometer

The quadrupole ITMS is a modified Thermo Finnigan LCQ classic (see Fig. 1). The last part of the ion optics (octupoles), the ion trap and the detection system (conversion dynode and electron multiplier) were not changed. The vacuum system was altered (a compact diaphragm forepump (Vacuubrand MZ4) was installed in front of the split flow turbo molecular pump (Balzers-Pfeiffer TMH 260-130)). The focussing of the ions from the ion flow reactor IFR towards the first pressure chamber of ITMS ($\approx 10^{-1}$ Pa) is a unique development by MPIK Heidelberg and is achieved by an ion cone with a critical orifice (d = 0.15 cm diameter) and a front electrode (0.15 mm diameter) just before the first octupole (both fabricated from stainless steel). The pressure in the pre-chamber containing the ion cone and front electrode is kept constant at a value $\leq 1 \times 10^4$ Pa using a pump. A flow is produced by this pump (rotary vane vacuum pump BUSCH RA 0025 E (543), alternatively a Ruvac WA 150 Roots pump together with an Alcatel ALCV 750 pump) and is controlled by the critical orifice. The standard flow Q_{IFR} (in standard liters per minute, slm, p_0= 1013 hPa, T_0= 273 K) through the critical orifice depends linearly on the pressure p (hPa) in front of it [30]:

$$Q_{\mathrm{IFR}} = \frac{0.93 s d^2 p T_0}{\sqrt{293 T_I}}, \tag{7}$$

with s: cut factor, d (cm): diameter of orifice and T_I (K): temperature at orifice. As s is not well known the flow is calibrated with the help of a thermal mass flow controller and a pressure sensor. A small part of this flow passes through the front electrode of ITMS. The voltages of the front electrode, the octupoles and the amplitude of the radio frequency (RF) of the octupoles are optimized with the help of the software Tune Plus (Thermo Finnigan). Typical values (V) are: front electrode: −1, octupole 1 offset: 4, interoctupole lens voltage: 9, octupole 2 offset: 11, octupole RF amplitude (Vp-p) 940.00. Because of the low mass cut off of the ion trap and the tuning of the voltages for the heavier product ions, the reagent ions can suffer from a mass discrimination. Due to the optimization of the ion optics for product ions the transmission for other ions can decrease. Ions with low masses that reach the ion trap despite this effect also suffer from a reduced stability inside the trap (compared to heavier ions) if their mass is close to the low mass cut off. These two effects are summarized in the so-called mass discrimination of ITMS. Correction factors ($\leq$2 at mass 125 amu relative to mass 160 amu) for this discrimination were derived from laboratory measurements (comparison of reagent ions intensities in and without presence of product ions). These correction factors are necessary especially if the calibration and/or atmospheric measurements are done at high ion intensity ratios (product ions/reagent ions) because $\ln(1+R)$ cannot be approximated by R in these cases.

The interoctupol lens open during an injection time of maximum 8 s to release the ions into the second pressure chamber ($\approx 3 \times 10^{-3}$ Pa). The actual injection time is about (6±2) s as an automatic gain control is activated during the measurements which allows only a certain (maximum) amount of ions entering the ion trap to prevent changes in the electrical fields inside the trap due to space charge effects. These changes may result in a decrease of the mass resolution. Due to the poor statistics of the ion counting during a single mass scan a preselected averaging over a certain amounts of so-called micro scans is activated (see Section 2.5).

2.4. Flow tubes

For the atmospheric measurements there are actually three different flows needed: Q_{blow} is driven by a blower and both Q_{SL} and Q_{IFR} by a pump. The flow Q_{IFR} that arrives at ITMS and the pump were already described in Section 2.3. The flow Q_{IFR} in IFR is the sum of sampled air Q_{SL} in SL and the carrier gas from IS (see Section 2.1). Another flow Q_{CS} is used for the calibration (see Section 2.5).

A guided inlet $\mathrm{Ft_{blow}}$ (diameter 0.2 m) is used for the atmospheric measurements of GSA and OH (see Fig. 1) with a high flow Q_{blow} = 1100 $\mathrm{m^3/h}$ produced by a blower (pipe ventilator, Maico EZR 20/2 B). From the central part of this flow an air column is sampled by the probe air inlet (stainless steel cone with an orifice diameter of 5 mm) into the sampling line SL. So it is assured that the probe air is not directly affected by walls or other obstacles close-by on the outside of the measurement building. The distance of the guided inlet from the roof/wall of the building is about 0.5 m ($\approx$ 0.3 m for the setup at UFS). The length of SL that is made out of QF40 stainless steel parts is about 1 m (0.4 m for the setup at UFS). During most of the measurements an inlet in the roof was chosen.

2.5. Calibration source

Though the rate coefficient of the applied detection reaction is relatively well known ((Eq. 6)), additional uncertainties because of H_2SO_4 wall losses in the sampling line and uncertain flow conditions in the ion flow reactor IFR exist. As the sampling line SL is made as short as possible (to minimize wall losses) and the injected carrier gas from the ion source has a higher velocity than the surrounding probe gas the ion residence time t_{ir} cannot be derived as exactly as it could be in an ideal laminar flow. Bending of IFR is even more critical for a calculation of t_{ir}. There are also uncertainties in mass discrimination of the reagent ions (see Section 2.3). Therefore a calibration source CS is needed which can be directly connected to the probe air inlet to have similar conditions as during atmospheric measurements (see Fig. 1).

A certain amount of OH radicals is produced by CS. The subsequent titration with $^{32}SO_2$ yields a corresponding amount of H_2SO_4 that is detected with ITCIMS. Different kinds of OH calibration techniques are described in [31] (and references given there) and [32]. The calibration of the measurements presented here is based on water vapor photolysis at a wavelength of 184.9 nm:

$$\mathrm{H_2O} + h\nu \rightarrow \mathrm{OH} + \mathrm{H} \quad (\nu = c/184.9\,\mathrm{nm}), \tag{8}$$

$$\mathrm{H} + \mathrm{O_2} + \mathrm{M} \rightarrow \mathrm{HO_2} + \mathrm{M}.$$

The production of H_2SO_4 from the reaction of SO_2 with the photolysis product OH and consecutive reactions occurs in the same way as in the atmosphere due to the Stockwell/Calvert mechanism (reactions (1)–(3)).

Table 1
Typical parameters calibration part

		Unit	δ(%)	
A	1.30×10^{-5}	m^2	[d]	Sensitive area of photodiode (Hamamatsu S1226-44BQ)
s_{185}	0.097	A/W	2.7	Spectral sensitivity of photodiode at 184.9 nm [a]
k_d	1.380		1.4	Correction factor – beam divergency [b]
k_T	1.293		0.8	Correction factor – transmission suprasil tube [b]
ρ	0.085		1.4	Reflectivity of suprasil tube [c]
k_L	1.078		5	Correction factor – length illumination zone [c,b]
σO_2	1.4×10^{-20}	cm^2	22	Absorption cross-section of O_2 [b] At 184.9 nm and O_2 column $\approx 5 \times 10^{18}$ cm^{-2}
σH_2O, *i*	7.14×10^{-20}	cm^2	2.8	Absorption cross-section of water vapor At 184.9 nm [48]
σH_2O, ii	7.22×10^{-20}	cm^2	3	At 184.9 nm [49]
b	1.5	cm	[d]	Width of aperture
Q_R	20–27	slm	3	Total flow through suprasil glass tube II
Q_r	13–18.5	slm	3	Taken flow from Q_R for flow tube I [b]
p	1×10^3	hPa	0.2	Pressure in tube I and at the end of tube II [b]
T	22	°C	0.3	Typical gas temperature at the end of tube II [b]
R	1.0	cm	[d]	Radius of suprasil tube
I	20 – 190	nA	1	Photo current [b]
$[H_2O]_0$	0.1–1.7	$10^{17}/cm^3$	4.3	water vapor concentration in tube II [b,c]

[a] Derived from a comparison measurement with a calibrated photodiode Hamamatsu G2119 from PTB, Berlin.
[b] Measured.
[c] Calculated.
[d] Error negligible.

The setup is shown in Fig. 1: Purified air is humidified to a certain amount (water vapor concentrations between $1 \cdot 10^{16}$ and $1.7 \cdot 10^{17}$ ♯/cm^3) and irradiated with UV-light (wavelength 184.91 nm) in a well-defined zone. The probe air inlet (the same as the one used during atmospheric measurements) sucks a fraction of this air containing OH radicals. To produce sulfuric acid, an inlet for a SO_2/N_2 gas flow (stainless steel, outer diameter 3 mm, (0.1–0.8) slm, (2–4) mmol/mol SO_2 in N_2 5.0) is positioned just after the probe air inlet cone in opposite flow direction to ensure a fast mixing with the probe air. A minimum gas flow ($\leq$ 0.1 slm) is chosen if one is sure that a higher gas flow would not lead to an increase in the sulfuric acid concentration.

The water vapor photolysis takes place in an homogeneously illuminated well defined zone under preferably well defined laminar gas flow conditions (Q_{CS}) inside tube Ft_{CS}. This zone is located at the end of Ft_{CS} inside a calibration unit. Ft_{CS} is made out of synthetic fused silica (Heraeus Suprasil, radius R = 1.0 cm). The length (which is critical for the formation of a laminar flow) was preferably chosen quite long (l= 1.5 m) and the flow (Q_{CS}= 20 slm) relatively low for the so-called laminar setup with a Reynolds number of $\approx$ 1500. For the OH and H_2SO_4 measurements at UFS (see Section 3.2) a quit short tube was chosen ($\approx$0.75 m) because of space limitations getting a turbulent flow (Q_{CS}= 27 slm) with a Reynolds number of $\approx$ 2000. This so-called turbulent setup requires more attention concerning the determination of the photon flux and the duration of the photolysis (see below), but this setup has no risk of an undefined (half laminar/half turbulent) flow which exists for in-between lengths of Ft_{CS}. A disadvantage of a turbulent flow are more wall losses of OH-radicals due to turbulent diffusion. The wall-losses of OH for this setup due to turbulent and molecular diffusion were empirically determined to be 10%.

The calibration unit consists of a lightproof case that contains an UV lamp, an optical system, a part of Ft_{CS} and a photodiode (see Fig. 3).

The production rate of OH (according to reaction (8)) is proportional to $[H_2O]$, the absorption cross section σ_{H_2O} of H_2O, the quantum yield $\Phi_{OH,185}$ and the photon flux Ψ. Integration yields the OH-concentration (Eq. (9)). For the laminar setup mean values for the photon flux $\overline{\Psi}_c$ and the duration of photolysis τ_c in the center of tube Ft_{CS} can be used (Eq. (10)). The irradiance determines $\overline{\Psi}_c$ (Eq. (11)). The irradiance is derived from the photo current I of a calibrated photodiode, divided by its spectral sensitivity s and sensitive area A. The photo current is measured with an electrometer (Keithley 6514). The photon flux $\overline{\Psi}_c$ is the irradiance divided by the photon energy $E = hc/\lambda$ times a correction term to obtain the photon flux in the center of the photolysis region. The length L of the illumination zone and the mean velocity of the sampled (calibration) flow Q_{SL} determine τ_c (Eq. (12)). L is determined by the geometry of the optical system (= $k_L \times$ width of aperture b).

$$\frac{d[OH]}{dt} = \{[H_2O]_0 - [OH]\}\sigma_{H_2O}\Phi_{OH,185}\Psi$$
$$\Phi_{OH,185} \approx 1 \ [33] \rightsquigarrow \quad (9)$$
$$[OH] \approx [H_2O]_0\sigma_{H_2O}\int_0^\tau \Psi dt \ ([OH] \ll [H_2O]_0)$$

$$\int_0^\tau \Psi dt = \overline{\Psi}_c\tau_c \ (\text{laminar setup}) \quad (10)$$

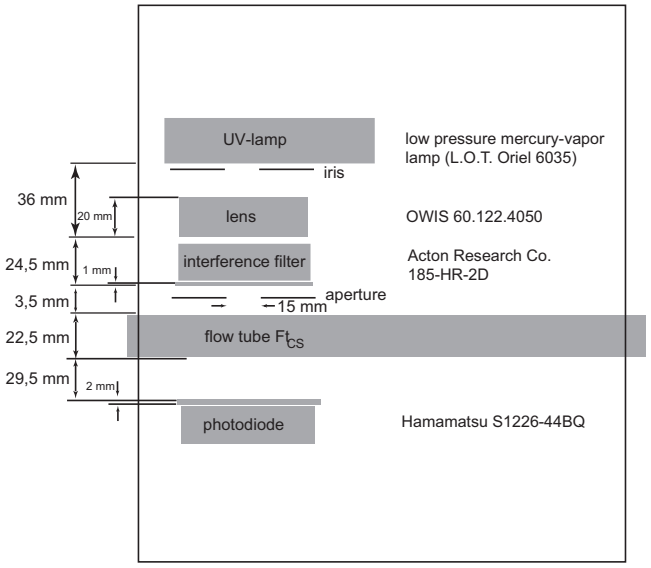

Fig. 3. Schematic of the optical system of the calibration unit as part of the calibration source (CS).

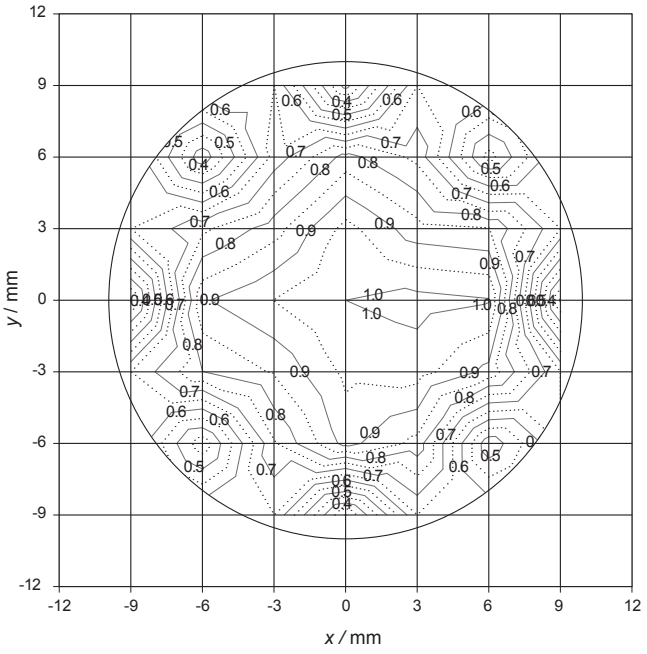

Fig. 4. HO_2-profile in tube Ft_{CS}: ratio between measured [35] and calculated HO_2 concentrations.

$$\overline{\Psi}_c = \frac{I}{sAE_{\text{photon}}} k_d k_T (e^{k_\sigma R} + \rho e^{-k_\sigma R}), \text{ (laminar setup)} \quad (11)$$

$$k_\sigma = (\sigma_{O_2}[O_2] + \sigma_{H_2O}[H_2O])$$

$$\tau_c = \frac{k_L b p T_0}{Q_r p_0 T} \pi r^2, \text{ (laminar setup)} \quad (12)$$

$$r^2 = R^2(1 - \sqrt{1 - Q_r/Q_R}),$$

r = radius of the calibration volume (cylinder).

For the laminar setup correction factors have been derived (k_L, k_d, k_T and ρ). For more details see Table 1.

For the turbulent setup the integral $\int_0^\tau \Psi dt$ cannot be simplified as in the laminar case (10), so the photon flux and the duration of photolysis had to be determined three dimensional by cylindrical coordinates.

The calibration unit is flushed by dry nitrogen to prevent absorption of the UV-light by ambient oxygen. The flow Q_{CS} inside tube Ft_{CS} contains oxygen and water vapor that absorb UV-light at the observed wavelength. The correction for this phenomena is due to Lambert–Beer law, so is the correction of the absorption of the reflected light from the tube's wall (Eq. (11)). The flow Q_{CS} is produced by a pure air generator (NBS 2000, company Breitfuss) and a humidification unit. The latter consists of a gas wash bottle filled with distilled water and additional empty bottles to prevent water droplets from bursted bubbles getting into Ft_{CS}. The dew point temperature of the humidified zero air is measured by an optical chilled mirror hygrometer (DewTrak 200, EdgeTech), alternatively with a thin-film aluminum oxide moisture sensor (AMX 1 Dew Point Transmitter, Panametrics). The water vapor concentration $[H_2O]_0$ is derived from the dew point temperature via an approximation formula [34]. The absorption of the UV-light (photon flux at $\lambda = 184.9$ nm during τ) by a known concentration of water molecules (with the absorption cross-section σ_{H_2O}) leads with the quantum yield $\Phi_{OH,185}$ to OH molecules. A part of the flow Q_{CS} is taken for the flow in SL. This part Q_{SL} has to be less than 70% of Q_{CS}. Otherwise the error of the calculated OH-concentration according to (Eq. (9)) becomes too large due to boundary effects. In

Fig. 5. Zugpitze: summit and Environmental Research Station Schneefernerhaus (UFS).

Fig. 4 the relative deviations of measured HO_2 concentrations [35] from comparable calculations of HO_2 production (of the same calibration source) are shown. For this purpose a small flow Q_{SL} was taken at different positions of the cross-section of Ft_{CS}.

The atmospheric GSA (OH) concentration is the product of a calibration factor (obtained from the calibration described above) and $\ln(1 + R_{160(162),125})$, with $R_{160(162),125}$: ratio of ion intensities at mass 160 (162) and mass 125. The systematic error of the calibration factor is ±25%. There is an additional statistical error due to the variation of the ion intensities measured by the mass spectrometer. The observed peak ion signal intensity is proportional to a peak ion count rate. However, the unit of this ion intensity is arbitrary for the used ITMS. The observed standard deviations of mean values from respective more than 20 single values of the ion intensities at mass 160 and 125 during a calibration showed that the chosen integration over 10 micro scans leads to a statistical error with an upper limit of about plus or minus 10% in the GSA (OH)-concentration range of the calibration unit (10^7–10^8 molecules per cm^3). To improve the precision for lower ambient GSA (OH) concentrations an integration of 30–50 micro scans is used during the atmospheric measurements in the planetary boundary layer. This leads to an accuracy of about plus or minus 30% in the upper 10^6 molecules per cm^3—range for both GSA and OH measurements (plus or minus 33 % or more for OH measurements because of interferences with HO_2, see Section 3.2). The precision is better than plus or minus 10% in this range.

Between the atmospheric measurements, background measurements for GSA and OH are performed. For GSA, the background is measured by exchanging the probe air inlet cone with a special fins-like construction out of stainless steel covered by several layers (up to 32) of relatively porous and absorbent laboratory paper. The background signal is subtracted from the signal at mass

Table 2
Parameters of OH/GSA-measurements at the mountain station Zugspitze October 2001.

Parameter		Unit
p	735	hPa
T_I	32	°C
$p_{\text{recipient}}$	95–97	hPa
Q_r	18.5	slm
Ion source	^{210}Po: 62	MBq
Detection limit OH (3σ)	$1.9 \cdot 10^5$	♯/cm^3
Detection limit GSA (3σ)	$1.2 \cdot 10^5$	♯/cm^3
Time resolution	140	s
Reaction gas for OH	2 mmol/mol $^{34}SO_2$ in N_2: 0.122, N_2: 0.44	slm slm

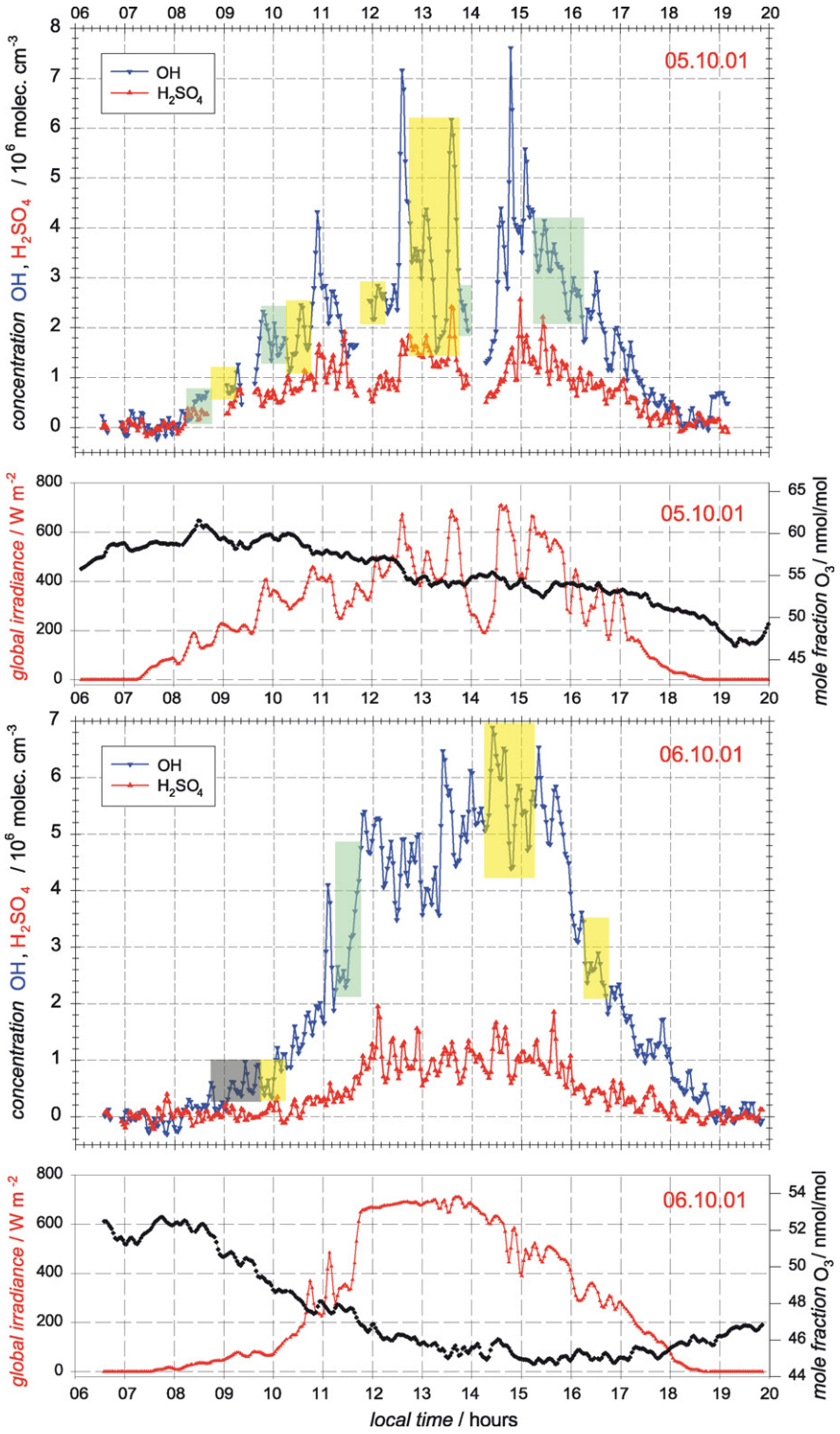

Fig. 6. Measured concentrations of OH and GSA, ozone and global irradiance (DWD) at mountainside Zugspitze (05. and 06.10.2001). The colored rectangles represent additional errors of the OH data (yellow: −24%, grey: −33%, green: undefined (see text)).

160 obtained during atmospheric measurements. For OH the background measurements are described in Section 3.2.

3. Atmospheric measurements

3.1. Gaseous sulfuric acid in the planetary boundary layer

We have deployed the ITCIMS instrument for many ground-based GSA measurements in the planetary boundary layer. Most of them took place in the framework of the EU-project QUEST (Quantification of Aerosol Nucleation in the European Boundary layer). All in all, data of several months have been obtained. They have been presented and interpreted focussing on new particle formation and growth [18,36–42]. New particle formation events observed, e.g., during QUEST III (Heidelberg) and IV (Hyytiälä, Finland) are studied in respect to the measured sulfuric acid concentrations in [40]. A correlation, e.g., of the time-shifted square of GSA concentrations with concentrations of N_{36} particles (with diameters

between 3 and 6 nm) is an implication for kinetic nucleation resulting in ammonium-bisulfate particles. The time-shift is reasonable because the N_{36} particles have already grown. Also correlations with [H_2SO_4] have been observed. An overview of connections between aerosol formation and sulfuric acid can be found in [43] and a summary of new particle formation studies that had simultaneous measurements of [H_2SO_4] is shown in [44].

There are recent implications [45] that the measured sulfuric acid is only a lower limit if strong base molecules like amines are present. The reason is that CIMS is less sensitive for amine-sulfuric acid clusters.

3.2. Gaseous sulfuric acid and hydroxyl radicals at the high-altitude mountain station Zugspitze

GSA and OH have been measured at the Schneefernerhaus UFS (2650 m asl, below the summit of Mount Zugspitze in the Bavarian Alps, Germany) in 2001 (during the field measurement campaigns 10.05.01–01.06.01 and 31.09.01–12.10.01). The UFS has the status of a global station within the Global Atmosphere Watch Programme of the World Meteorological Organization (WMO). It is located ≈ 310 m below the summit of Zugspitze at its southern slope (see Fig. 5). The air masses came mostly out of west from the Schneefernerscharte between the summits of Schneefernerkopf (at the very left side of Fig. 5) and Zuspitze.

Exemplary, two days are presented in the following (05. and 06.10.2001). On the first day, air masses were predominantly of free troposphere origin (backward trajectories from National Oceanic and Atmospheric Administration (NOAA) and British Atmospheric Data Centre (BADC)) and it was a cloudy day. The second day was almost cloud-free in the second half and the air masses came more and more from the boundary layer. But the SO_2 measurements of another CIMS instrument (MPIK, [46,47]) showed no convection of SO_2-rich boundary air (mean values less than 20 pmol/mol). Presumably an inversion over the valley occurred. A significant change in the meteorology occurred at approximately 13:22. The wind changed its direction from west to southeast (foehn) and the air masses came from the area of the Alps.

For the atmospheric OH measurements, titration of OH in $H_2{}^{34}SO_4$ in less than 30 ms was done just behind the probe air inlet (see Fig. 1). The required concentration of isotopically labeled SO_2 (Linde, 2 mmol/mol SO_2 in N_2, ≈92% $^{34}SO_2$, flows see Table 2) has been determined empirically and via a kinetic simulation [29]. For background measurements NO_2 was added to the $N_2/^{34}SO_2$ mixture to quench the atmospheric OH. The mole fraction of NO_2 just behind the inlet was 65.5 μmol/mol during these measurements that were repeated several times. Additional background measurements as described in Section 2.5 were done. Interferences between H_2SO_4 with OH because of the natural and artificial distributions of the isotopes were corrected.

Interferences of OH measurements with HO_2 because of reactions with NO and O_3 have been considered and lead to a slightly degraded accuracy of about ±33% for NO values below 40 pmol/mol (HO_2 was estimated to be between 5 and 20 pmol/mol, wall losses of HO_2 have been determined empirically and considered). For higher NO mole fractions (measured by the Umweltbundesamt at the mountain top) the (negative) accuracy gets worse corresponding to Fig. 6 (because of the low time resolution of the NO data (30 min) only the maximum values of two mole fraction intervals (40–80 pmol/mol and 80–120 pmol/mol) have been considered for the error estimations). Because of the lack of a few NO data the corresponding (negative) accuracies of the OH data are undefined. An extension of the OH measurement will be the quenching of HO_2 inside SL to minimize such interferences, e.g., with the help of NO_2 just after the titration region of the probed ambient atmospheric OH.

Both measured concentrations of GSA and OH show a diurnal variation and a good correlation with the global irradiance measured by the DWD (Deutscher Wetterdienst) (see Fig. 6). Especially the variations at lower time scales due to clouds (05.10.01) are reflected in the OH but also in the GSA concentrations. Maximum concentrations of GSA and OH of 2.6×10^6 and 7.6×10^6 molecules/cm^3, respectively, were observed. Mean values of OH at noon were ≈3.5×10^6 (05.10.01) and 4.5×10^6 molecules/cm^3 (06.10.01).

The detection limit of OH was 1.9×10^5 molecules/cm^3 (3×10^5 molecules/cm^3 before 8:10 on 05.10.), for H_2SO_4 1.2×10^5 molecules/cm^3 (2×10^5 molecules/cm^3 before 8:10 on 05.10.) (time resolution 140 s).

The accuracy for OH was for 6×10^6 molecules/cm^3 ±33%, for 6×10^5 molecules/cm^3 ±48% (NO below 40 pmol/mol). The accuracy for H_2SO_4 was found to be at typical values of 1×10^6 molecules/cm^3 ±36%.

4. Summary and conclusions

The ITCIMS instrument has been successfully deployed for GSA measurements in the planetary boundary layer and for simultaneous measurements of GSA and OH at the high-altitude mountainside Zugpitze. First conclusions regarding the influence on new particle formation have been drawn from the GSA measurements (see references in Section 3.1). Further measurements of GSA, ammonia and amines in the future are important, not only measurements at ground-level but also ship and aircraft borne measurements. Ammonia and amines can also be measured via CIMS in the positive ion mode due to their large proton affinities. Measurements above the planetary boundary layer have the advantage that due to lower humidity the sensitivity of ITMS increases and thus a higher time resolution can be chosen. The lower temperatures prevailing above the boundary layer promote nucleation, provided that nucleating gases are sufficiently abundant.

Acknowledgements

Parts of this work were funded by the EU-project QUEST and by a BMBF (Federal Ministry of Education and Research) PhD scholarship. The measurements at the UFS Schneefernerhaus were performed in the frame of the SCAVEX (Charakterisierung von Aerosolen und anthropogenen Stickoxiden in Bezug auf Klimawirksamkeit und Luftchemie) project funded in part by the Bayerisches Staatministerium für Umwelt, Gesundheit und Verbraucherschutz.

References

[1] V.-M. Kerminen, H. Lihavainen, M. Komppula, Y. Viisanen, M. Kulmala, Geophys. Res. Lett. 32 (2005) L14803, doi:10.1029/2005GL023130.
[2] A. Laaksonen, A. Hamed, J. Joutsensaari, L. Hiltunen, F. Cavalli, W. Junkermann, A. Asmi, S. Fuzzi, M.C. Facchini, Geophys. Res. Lett. 32 (2005) L06812, doi:10.1029/2004GL022092.
[3] D.A. Hegg, M.B. Baker, Rep. Prog. Phys. 72 (2009) 056801, doi:10.1088/0034-4885/72/5/056801.
[4] T. Kurtén, V. Loukonen, H. Vehkamäki, M. Kulmala, Atmos. Chem. Phys. 8 (2008) 4095–4103, doi:10.5194/acp-8-4095-2008.
[5] M.B. Enghoff, H. Svensmark, Atmos. Chem. Phys. 8 (2008) 4911–4923, doi:10.5194/acp-8-4911-2008.
[6] A. Sorokin, F. Arnold, D. Wiedner, Atmos. Environ. 40 (2006) 2030–2045, doi:10.1016/j.atmosenv.2005.11.053.
[7] W.R. Stockwell, J.G. Calvert, Atmos. Environ. 17 (1983) 2231–2235, doi:10.1016/0004-6981(83)90220-2.
[8] T. Reiner, F. Arnold, Geophys. Res. Lett. 20 (1993) 2659–2662, doi:10.1029/93GL02996.
[9] T. Reiner, F. Arnold, J. Chem. Phys. 101 (1994) 7399–7407, doi:10.1063/1.468298.
[10] C.E. Kolb, J.T. Jayne, D. Worsnop, M.J. Molina, R.F. Meads, A.A. Viggiano, J. Am. Chem. Soc. 116 (1994) 10314–10315, doi:10.1021/ja00101a067.
[11] E.R. Lovejoy, D.R. Hanson, L.G. Huey, J. Phys. Chem. 100 (1996) 19911–19916, doi:10.1021/jp962414d.

[12] J.H. Seinfeld, S.N. Pandis, in: Atmospheric Chemistry and Physics. From Air Pollution to Climate Change, Wiley, USA, 1998.
[13] F. Arnold, R. Fabian, Nature 283 (1980) 55–57, doi:10.1038/283055a0.
[14] F. Arnold, T. Bührke, Nature 301 (1983) 293–295, doi:10.1038/301293a0.
[15] O. Möhler, F. Arnold, Geophys. Res. Lett. 19 (1992) 1763–1766, doi:10.1029/92GL01807.
[16] F. Eisele, D. Tanner, J. Geophys. Res. 98 (1993) 9001–9010, doi:10.1029/93JD00031.
[17] H. Berresheim, T. Elste, C. Plass-Dülmer, F.L. Eisele, D.J. Tanner, Int. J. Mass spectrom. 202 (2000) 91–109, doi:10.1016/S1387-3806(00)00233-5.
[18] V. Fiedler, M.D. Maso, M. Boy, H. Aufmhoff, J. Hoffmann, T. Schuck, W. Birmili, M. Hanke, J. Uecker, F. Arnold, M. Kulmala, Atmos. Chem. Phys. 5 (2005) 1773–1785, doi:10.5194/acp-5-1773-2005.
[19] F. Arnold, L. Pirjola, H. Aufmhoff, T. Schuck, T. Lähde, K. Hämeri, Atmos. Environ. 40 (2006) 7097–7105, doi:10.1016/j.atmosenv.2006.06.038.
[20] T. Petäjä, R.L. Mauldin III, E. Kosciuch, J. McGrath, T. Nieminen, P. Paasonen, M. Boy, A. Adamov, T. Kotiaho, M. Kulmala, Atmos. Chem. Phys. 9 (2009) 7435–7448, doi:10.5194/acp-9-7435-2009.
[21] M. Speidel, R. Nau, F. Arnold, H. Schlager, A. Stohl, Atmos. Environ. 41 (2007) 2427–2437, doi:10.1016/j.atmosenv.2006.07.047.
[22] V. Fiedler, R. Nau, S. Ludmann, F. Arnold, H. Schlager, A. Stohl, Atmos. Chem. Phys. 9 (2009) 4717–4728, doi:10.5194/acp-9-4717-2009.
[23] A. Roiger, H. Aufmhoff, P. Stock, F. Arnold, H. Schlager, Atmos. Meas. Technol. 4 (2011) 173–188, doi:10.5194/amt-4-173-2011.
[24] A. Kiendler, S. Aberle, F. Arnold, Atmos. Environ. 34 (2000) 2623–2632, doi:10.1016/S1352-2310(99)00475-6.
[25] F.C. Fehsenfeld, J.H. Carleton, A.L. Schmeltekopf, J. Chem. Phys. 63 (1975) 2835–2841, doi:10.1063/1.431722.
[26] O. Möhler, F. Arnold, J. Atmos. Chem. 13 (1991) 33–61, doi:10.1007/BF00048099.
[27] A.A. Viggiano, J.V. Seeley, P.L. Mundis, J.S. Williamson, R.A. Morrison, J. Phys. Chem. A 101 (1997) (1768) 8275–8278, doi:10.1021/jp97.
[28] D.J. Tanner, F.L. Eisele, J. Geophys. Res. 100 (1995) 2883–2892, doi:10.1029/94JD02609.
[29] J. Uecker, Measurements of the atmospheric radicals OH, HO_2 RO_2 as well as the ultra trace gas H_2SO_4—further development, calibration and deployment of a highly sensitive mass-spectrometric analytic method, Ph.D. thesis, University of Heidelberg, 2002.
[30] M. Wutz, H. Adam, W.W. (Ed.), Theorie und Praxis der Vakuumtechnik, Vieweg, Braunschweig; Wiesbaden, 1992.
[31] S. Dusanter, D. Vimal, P.S. Stevens, Atmos. Chem. Phys. 8 (2008) 321–340, doi:10.5194/acp-8-321-2008.
[32] A. Kukui, G. Ancellet, G.L. Bras, J. Atmos. Chem. 61 (2008) 133–154, doi:10.1007/s10874-009-9130-9.
[33] L.J. Stief, W.A. Payne, R.B. Klemm, J. Chem. Phys. 62 (1975) 4000–4008, doi:10.1063/1.430323.
[34] P.R. Wiederhold, in: Water Vapor Measurements: Methods and Instrumentation, Marcel Dekker Inc., New York, 1997.
[35] M. Hanke, J. Uecker, T. Reiner, F. Arnold, Int. J. Mass spectrom. 213 (2002) 91–99, doi:10.1016/S1387-3806(01)00548-6.
[36] M. Boy, M. Kulmala, T.M. Ruuskanen, M. Pihlatie, A. Reissell, P.P. Aalto, P. Keronen, M. Dal Maso, H. Hellen, H. Hakola, R. Jansson, M. Hanke, F. Arnold, Atmos. Chem. Phys. 5 (2005) 863–878, doi:10.5194/acp-5-863-2005.
[37] M. Ehn, T. Petäjä, H. Aufmhoff, P. Aalto, K. Hämeri, F. Arnold, A. Laaksonen, M. Kulmala, Atmos. Chem. Phys. 7 (2007) 211–222, doi:10.5194/acp-7-211-2007.
[38] M. Kulmala, K.E.J. Lehtinen, A. Laaksonen, Atmos. Chem. Phys. 6 (2006) 787–793, doi:10.5194/acp-6-787-2006.
[39] L. Laakso, T. Anttila, K.E.J. Lehtinen, P.P. Aalto, M. Kulmala, U. Hørrak, J. Paatero, M. Hanke, F. Arnold, Atmos. Chem. Phys. 4 (2004) 2353–2366, doi:10.5194/acp-4-2353-2004.
[40] I. Riipinen, S.-L. Sihto, M. Kulmala, F. Arnold, M. Dal Maso, W. Birmili, K. Saarnio, K. Dal Maso, K. Teinilä, V.-M. Kerminen, A. Laaksonen, K.E.J. Lehtinen, Atmos. Chem. Phys. 7 (2007) 1899–1914, doi:10.5194/acp-7-1899-2007.
[41] S.-L. Sihto, M. Kulmala, V.-M. Kerminen, M. Dal Maso, T. Petäjä, I. Riipinen, H. Korhonen, F. Arnold, R. Janson, M. Boy, A. Laaksonen, K.E.J. Lehtinen, Atmos. Chem. Phys. 6 (2006) 4079–4091, doi:10.5194/acp-6-4079-2006.
[42] A. Laaksonen, M. Kulmala, T. Berndt, F. Stratmann, S. Mikkonen, A. Ruuskanen, K.E.J. Lehtinen, M. Dal Maso, P. Aalto, T. Petäjä, I. Riipinen, S.-L. Sihto, R. Janson, F. Arnold, M. Hanke, J. Ücker, B. Umann, K. Sellegri, C.D. O'Dowd, Y. Viisanen, Atmos. Chem. Phys. 8 (2008) 7255–7264, doi:10.5194/acp-8-7255-2008.
[43] M. Kulmala, V.-M. Kerminen, Atmos. Res. 90 (2008) 132–150, doi:10.1016/j.atmosres.2008.01.005.
[44] M.E. Erupe, D.R. Benson, J. Li, L.-H. Young, B. Verheggen, M. Al-Refai, O. Tahboub, V. Cunningham, F. Frimpong, A.A. Viggiano, S.-H. Lee, J. Geophys. Res. 115 (2010), doi:10.1029/2010JD013942.
[45] T. Kurtén, T. Petäjä, J. Smith, I.K. Ortega, M. Sipilä, H. Junninen, M. Ehn, H. Vehkamäki, L. Mauldin, D.R. Worsnop, S.-M. Kulmala, Atmos. Chem. Phys 11 (2011) 3007–3019, doi:10.5194/acp-11-3007-2011.
[46] M. Hanke, B. Umann, J. Uecker, F. Arnold, H. Bunz, Atmos. Chem. Phys. 3 (2003) 417–436, doi:10.5194/acp-3-417-2003.
[47] B. Umann, F. Arnold, C. Schaal, M. Hanke, J. Uecker, H. Aufmhoff, Y. Balkanski, R. Van Dingenen, J. Geophys. Res. 110 (2005) D22306, doi:10.1029/2005JD005906.
[48] C.A. Cantrell, A. Zimmer, G.S. Tyndall, Geophys. Res. Lett. 24 (1997) 2195–2198, doi:10.1029/97GL02100.
[49] D.J. Creasey, D.E. Heard, J.D. Lee, Geophys. Res. Lett. 27 (2000) 1651–1654, doi:10.1029/1999GL011014.